Ultrasound in Med. & Biol., Vol. 48, No. 7, pp. 1348–1355, 2022

0301-5629/$ - see front matter

https://doi.org/10.1016/j.ultrasmedbio.2022.02.024

● *Clinical Note*

# *B/A* MEASUREMENT OF CLEAR CELL RENAL CELL CARCINOMA VERSUS HEALTHY KIDNEY TISSUE

Anastasiia Panfilova,* Xufei Chen,* Christiaan Widdershoven,† Jan Erik Freund,‡ Dilara Savci Heijink,‡ Patricia Zondervan,† Ruud J.G. van Sloun,* Oleg A. Sapozhnikov,§,¶ Hessel Wijkstra,*,† and Massimo Mischi*

* Electrical Engineering Department, Faculty of Electrical Engineering, Eindhoven University of Technology, Eindhoven, The Netherlands; † Department of Urology, Amsterdam University Medical Centers, Location AMC, Amsterdam, The Netherlands; ‡ Department of Pathology, Amsterdam University Medical Centers, Location AMC, Amsterdam, The Netherlands; § Department of Acoustics, Physics Faculty, Moscow State University, Moscow, Russia; and ¶ Center for Industrial and Medical Ultrasound, Applied Physics Laboratory, University of Washington, Seattle, Washington, USA

(*Received* 21 *July* 2021; *revised* 16 *February* 2022; *in final form* 28 *February* 2022)

**Abstract—The acoustic parameter of non-linearity *B/A* has been found capable of discriminating some types of pathological tissue from healthy tissue. The literature on the utility of *B/A* for cancer diagnostics is very limited, with measurements on the human breast and liver. This work expands the current research on cancer diagnostics by *B/A* assessment of eight slices of human clear cell renal cell carcinoma (ccRCC) from two patients and four slices of healthy kidney tissue from two healthy kidney samples. The Wilcoxon test identified the *B/A* distribution of malignant tissue as not significantly different from that of healthy tissue. An alternative way of defining outliers resulted in median *B/A* values of 8.1 for ccRCC and 6.8 for healthy tissue ($p < 0.05$). Acoustic attenuation at 2.1 MHz was significantly greater ($p < 0.05$) for ccRCC (1.7 dB/cm) than for healthy tissue (1.0 dB/cm). The observed differences in the measured values suggest that *B/A* and acoustic attenuation may represent potential diagnostic markers of ccRCC. More data and an improved experimental design are required to provide a definitive conclusion on the utility of *B/A* for cancer diagnostics. (E-mail: anastasiapanfilova09@gmail.com)** 

***Key Words:*** **Non-linear parameter B/A, Cancer diagnostics, Ultrasound, *B/A* measurement.**

## INTRODUCTION

The ultrasound parameter of non-linearity *B/A* has been reported to reflect the water, fat and protein content of tissue (Apfel 1986; Sehgal et al. 1986). At the same time, *B/A* is also influenced by tissue structure: at equivalent chemical content, *B/A* has been found to decrease when cell-to-cell adhesion bonds are destroyed (Zhang et al. 1991). Cancerous tissue often exhibits altered water (Penet et al. 2021) and glycogen and lipid (Moch et al. 2016) content compared with healthy tissue, as is reported for human clear cell renal cell carcinoma (ccRCC). Moreover, cancerous tissue structure is characterized by increased cellularity (Moch et al. 2016) and lack of cell-to-cell adhesion (Janiszewska et al. 2020). Therefore, *B/A* may be a useful diagnostic parameter for cancer detection.

Whereas *B/A* clearly differentiates between healthy and diseased animal tissues (Zhang and Gong 1999; Wang et al. 2003), *B/A* measurements on cancerous human tissue have been performed only on liver and breast tissues (Sehgal et al. 1984, 1986). To further investigate the utility of *B/A* for cancer diagnostics, we measure *B/A* in the ex vivo setting of two healthy kidney specimens and two specimens of clear cell renal cell carcinoma (ccRCC), which is the most frequent renal carcinoma (Moch et al. 2016).

Address correspondence to: Anastasiia Panfilova, Eindhoven University of Technology, PO Box 513, Eindhoven, MB 5600, The Netherlands. E-mail: anastasiapanfilova09@gmail.com

## METHODS

### *Theoretical and experimental background*

As a sonic wave propagates, energy is transferred from the fundamental to higher harmonics. For

equivalent sonication conditions (source pressure and frequency), the amplitude of the second harmonic at a given distance from the source increases with the *B/A* value of the propagation medium (Gong et al. 1989). If the second harmonic is measured in water, the *B/A* of which is well known, and another measurement is made with the investigated sample inserted in the path between the source and receiver, the *B/A* of the studied sample can be determined from the ratio of the second harmonics in these two configurations (Gong et al. 1989). This strategy is called the finite-amplitude insert-substitution method (FAIS) (Gong et al. 1989). Like most finite amplitude methods based on the Fubini solution (Jafarzadeh et al. 2021), the FAIS assumes a plane monochromatic wave, the quasilinear condition and zero source non-linearity. In addition, it also makes the assumptions of a nearly linear frequency dependence of the sample attenuation coefficient and of the sample position being close to the receiver (Gong et al. 1989). In this work, we use the generalized FAIS method described in Panfilova et al. (2020), which removes the latter two assumptions.

To estimate *B/A*, besides measuring the second harmonic amplitudes, it is also necessary to measure the density $\rho$, the speed of sound $c$ and the attenuation coefficients at the fundamental and second harmonic frequencies $\alpha_1$and $\alpha_2$ of the sample. In this work, we follow the same measurement strategy as in Panfilova et al. (2020) but the tissue cuvette is made from steel, has a 4.5-cm-long base and is fixed on rails to ensure a stable position with cuvette sides strictly perpendicular to the beam propagation direction. All the quantities measured with the generalized FAIS (Panfilova et al. 2020) provide a single-value assessment corresponding to the studied region of the sample and disregarding the variation of these quantities within this region (Gong et al. 1989; Panfilova et al. 2020).

*Patient selection and sample preparation*

Two patients diagnosed with ccRCC and scheduled for radical nephrectomy provided oral consent to use the resected tissue for scientific purposes. After surgery, part of the cancerous tissue was selected by the histopathologist for the *B/A* measurement. After the measurement, the studied tissue was fixed and underwent histopathological analysis, confirming the diagnosis of ccRCC (sample 1: World Health Organization [WHO] grade 4, sample 2: WHO grade 3). Because of the smaller size of one of the tumors, a sample of healthy tissue was also available from one of the patients. To acquire more data for the healthy kidney, a specimen was selected on autopsy of a participant who donated his or her organs to science. An additional measurement on two porcine fat slices was performed for validation purposes.

The tissue was frozen for 1 h at −20°C to increase its stiffness and allow for an easier slicing procedure. To cut the kidney into slices with flat parallel sides, a dedicated device was used, as described in Panfilova et al. (2020). All slices were cut to a thickness of 4−7 mm. The two tumor samples provided three and five slices, respectively. Two healthy slices were available from one of the resected kidneys, and two more from the kidney extracted at autopsy.

*Measurement procedure*

The setup includes two circular flat (unfocused) single-element immersion transducers, the source C304-SU (251 Olympus NDT Inc., Waltham, MA, USA), with a nominal central frequency of 2.25 MHz, and the receiver V309 (Panametrics-NDT, 251 Olympus NDT Inc.), with a nominal central frequency of 5 MHz. The transducers were separated by a distance of 4.5 cm (Fig. 1). If we assume that the effective radius of the source is equal to its geometrical radius, the plane wave approximation is valid up to a distance of about 7 cm away from the source, constituting three-tenths of the length of the near field (Fig. 9 in Muir and Carstensen 1980). The distance between the source and the receiver has been chosen to be within this range and has been found suitable in the study that validated the generalized FAIS experimentally (Panfilova et al. 2020). The alignment of the source and the receiver was provided with a rail system, previously used in Panfilova et al. (2020). A steel cuvette fixing the tissue slices consisted of two parts: one attached to the receiver holder, and another fixed on the rails. Both sides of the cuvette had circular openings 30 mm in diameter, allowing the acoustic beam to pass. A system of rings inserted into both of the cuvette sides fixed to them a thin, acoustically transparent film (3-IN-1 FOLIE, Albert Hein B.V., Zaandam, Netherlands), which gently squeezed the tissue to ensure smooth surfaces.

Signal transmission and acquisition were controlled by LabVIEW (National Instruments Corp., Austin, TX, USA) software as previously described in Panfilova et al. (2020). The driving signals were 20-cycle tone bursts with a rectangular envelope generated by a 33220A arbitrary wave generator (Agilent Technologies, Santa Clara, CA, USA) and amplified by a 50-dB 2100L RF power amplifier (Acquitek, Massy, France) before transmission to the source transducer. For every acquisition, a total of 92−95 pulses were transmitted, received and saved.

The setup was submerged in a de-gassed water bath. The tissue slice was fixed between the cuvette sides under water to avoid trapping of air bubbles. Four through-transmission measurements were performed: two of low amplitude and two of high amplitude.

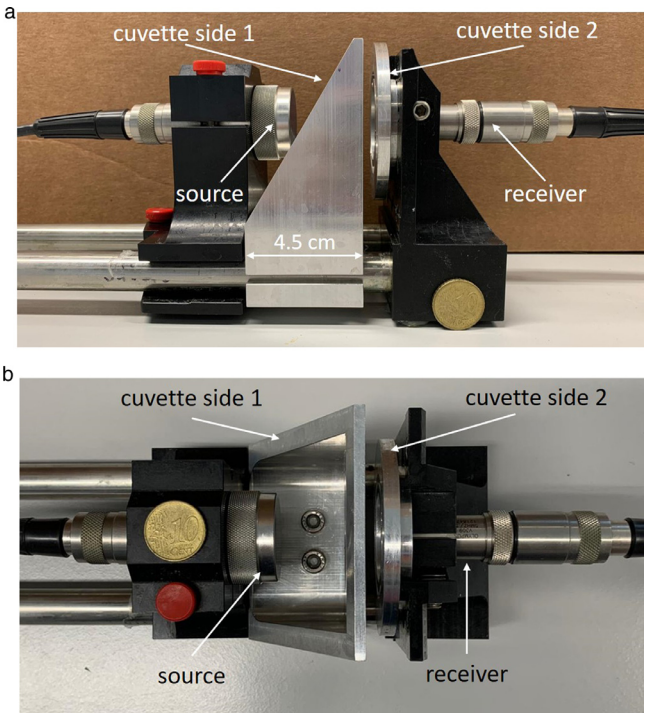


Fig. 1. (a) Side view of the measurement setup. (b) Top view of the measurement setup.

The two low-amplitude measurements involved the transmission of low-amplitude signals (<0.02 V) to the source at $f = 2.1$ MHz and $2f = 4.2$ MHz, aimed at determining $\alpha_1$ and $\alpha_2$. These signals resulted in a second harmonic level constituting only 0.004% of the fundamental, which allows assumption of the linear regime of sonic propagation, as required for attenuation measurements (Zeqiri et al. 2015).

Two high-amplitude measurements, transmitting 0.15 and 0.2 V to the source at $f$ were conducted to achieve second harmonic generation and register a second harmonic signal with a signal-to-noise ratio >30, yielding two *B/A* estimations. The received second harmonic amplitude constituted 4% and 5% of the fundamental, whereas the third harmonic component constituted 0.004% and 0.005% for the transmit amplitudes of 0.15 and 0.2 V, respectively. Such low higher harmonic amplitudes confirmed the validity of the Fubini solution (Duck 2002) and ensured compliance with the quasilinear condition. The signals for these sonication conditions were also previously recorded at a distance of 1.2 cm from the source, indicating higher harmonics below noise level; this supports the hypothesis that the source did not introduce non-linearity to the transmitted signal.

Once the low-amplitude and high-amplitude measurements described above were conducted, the tissue was flipped and the acquisition was performed again. Finally, the tissue was gently removed, keeping the sides of the cuvette in place, and the measurements were repeated without the sample. As a result, each tissue slice was measured in two orientations at two pressure amplitudes. Sample density $\rho$ was measured by weighing the slices on a H4J Pocket Weegschaal scale, where their volume is measured as the amount of displaced water in a Fisherbrand graduated cylinder.

*Data analysis*

The data were analyzed with MATLAB (The MathWorks, Inc., Natick, MA, USA). The speed of sound $c$ was determined based on the delay of the arrival time of the signal caused by the inserted sample with respect to water, determined by the maximum of the cross-correlation of the signals without and with the sample.

The fast Fourier transform was used to extract the amplitude of the fundamental frequency components of the low-amplitude pulses. The attenuation coefficients $\alpha_1$ and $\alpha_2$ were estimated based on the damping of the signal introduced by the sample, as in Panfilova et al. (2020).

When extracting the second harmonic amplitudes of the high-amplitude acquisitions, a Hanning window was used on all pulses fed to the fast Fourier transform to reduce spectral leakage from the strong fundamental component to the weaker second harmonic, as in Panfilova et al. (2020).

The Wilcoxon non-parametric test (Woolson 2007) was performed on B/A, c, $\alpha_1$ and $\alpha_2$ distributions to

identify if the difference between the median values of cancer and healthy tissue were significant. The *B/A* of biological tissue is known to be in the range from 5.2, corresponding to the *B/A* of water, to 11.3, corresponding to the highest value for fat (Panfilova et al. 2021a). Therefore, the values that are outside this range, accounting for the uncertainty of the measurement, have been disregarded as clearly erroneous. All data were included in the statistical analysis of $c$, $\alpha_1$ and $\alpha_2$.

*Measurement uncertainty*

A random uncertainty of 0.5% was estimated for the measured speed of sound, derived from the smallest possibly registered difference in the arrival times of two signals, defined by the sampling interval. A random uncertainty of 1% was estimated for the measured tissue density, based on the work of Law et al. (1985). The uncertainties in the measured distances between the source and the front face of the tissue sample and from the tissue rear face to the receiver (Fig. 1 in Panfilova et al. 2020) were estimated to be 0.02 cm. The uncertainty of the sample thickness was estimated to be 0.03 cm. The uncertainties of the second and fundamental harmonic component amplitudes were derived from the corresponding standard deviations among the recorded pulses for every acquisition separately (eqn 4 in Meyer 1989). The uncertainty in the attenuation coefficients was calculated according to Meyer (1989), deriving the partial derivatives of the attenuation coefficient with respect to all measured parameters, at the 68% confidence level. The same procedure (Meyer 1989) was performed to calculate the uncertainty of *B/A* for every measurement at the 68% confidence level, assuming the dependencies of all the aforementioned sources of uncertainty to be negligible. A 2% systematic error resulting from diffraction effects has been added to the estimated uncertainty of B/A, according to Gong et al. (1989).

## RESULTS

The measured *B/A* values for the two porcine fat slices are outlined in Table 1, revealing a maximum deviation of 13% from the literature value of 10.8 (Gong et al. 1989).

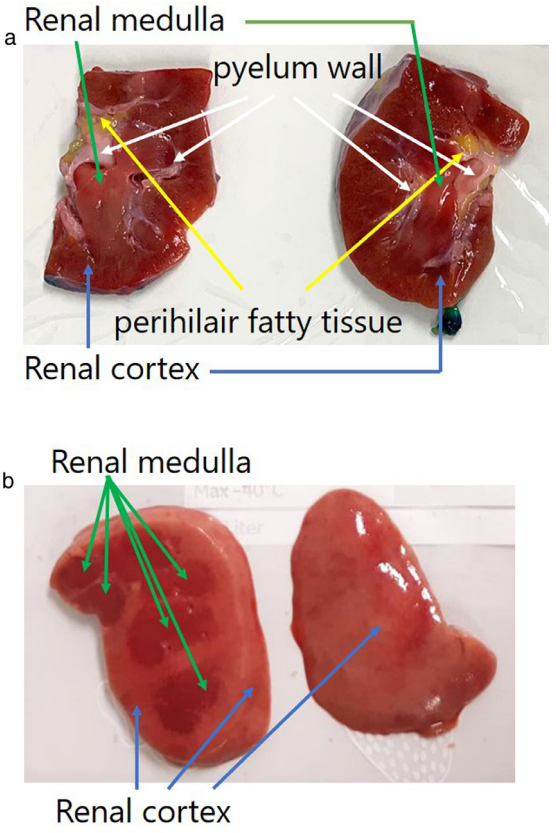


Fig. 2. (a) Slices of the remaining healthy kidney tissue from the first excised kidney. (b) Slices of the healthy kidney tissue taken at autopsy.

The studied human healthy kidney slices are illustrated in Figure 2, while the measured *B/A* values for these slices are listed in Table 2. The white pyelum wall structures in Figure 2a are stiff, owing to the higher stromal and muscular composition of the tissue, and may be expected to have acoustic properties different from those of the surrounding tissue. The yellow perihilar fatty tissue is expected to have a *B/A* close to 10.8, almost twice as high as that of the kidney parenchyma (Gong et al. 1989), as typical for fatty tissue.

In Figure 3 (a, b) are examples of the slices of the two tumor samples, revealing that tumor tissue is heterogeneous. Table 3 lists the measured acoustic parameters

Table 1. Measured acoustic parameters of two homogeneous slices of porcine fat

| Fat sample | | *B/A** | $c$ | $\alpha_1$(dB/cm) | $\alpha_2$(dB/cm) |
|---|---|---|---|---|---|
| Slice | Orientation | | | | |
| 1 | 1 | 11.1 ± 1.5, 12.0 ± 1.4 | 1531 ± 8 | 3.8 ± 0.2 | 10.4 ± 0.5 |
| 1 | 2 | 11.2 ± 1.4, 12.2 ± 1.4 | 1538 ± 8 | 3.8 ± 0.2 | 9.7 ± 0.4 |
| 2 | 1 | 10.6 ± 1.5,11.1 ± 1.4 | 1512 ± 8 | 4.5 ± 0.2 | 12.3 ± 0.5 |
| 2 | 2 | 11.3 ± 1.4, 10.6 ± 1.3 | 1509 ± 8 | 4.5 ± 0.2 | 12.2 ± 0.5 |

* The two *B/A* values in each column correspond to two high-amplitude acquisitions.

Table 2. Measured acoustic parameters of the healthy tissue slices

| Healthy kidney sample | | | *B/A** | *c* | $\alpha_1$(dB/cm) | $\alpha_2$(dB/cm) |
|---|---|---|---|---|---|---|
| Tumor | Slice | Orientation | | | | |
| 1 | 1 | 1 | **3.3 ± 2.7,**† 2.3 ± 2.6 | **1606 ± 8** | **4.5 ± 0.3** | **12.7 ± 0.8** |
| 1 | 1 | 2 | 22.3 ± 2.1, 21.5 ± 2.1 | **1636 ± 8** | **0.7 ± 0.0** | **5.4 ± 0.3** |
| 1 | 2 | 1 | **12.0 ± 1.5, 10.3 ± 1.4** | **1561 ± 8** | **1.1 ± 0.1** | **4.0 ± 0.3** |
| 1 | 2 | 2 | 2.7 ± 1.0, 3.2 ± 1.0 | **1566 ± 8** | **0.9 ± 0.1** | **2.6 ± 0.2** |
| 2 | 1 | 1 | **7.3 ± 0.8, 7.4 ± 0.8** | **1556 ± 8** | **1.3 ± 0.1** | **2.1 ± 0.1** |
| 2 | 1 | 2 | **7.8 ± 0.8, 8.1 ± 0.8** | **1544 ± 8** | **1.3 ± 0.1** | **2.1 ± 0.1** |
| 2 | 2 | 1 | **5.9 ± 1.3, 6.3 ± 1.3** | **1592 ± 8** | **0.8 ± 0.1** | **2.1 ± 0.1** |
| 2 | 2 | 2 | **5.4 ± 1.4, 5.2 ± 1.4** | **1538 ± 8** | **0.5 ± 0.0** | **1.2 ± 0.1** |

* The two *B/A* values in each column correspond to two high-amplitude acquisitions.
† Acquisitions that were included in the statistical analysis are presented in boldface.

of all investigated slices. The data included in the statistical analysis are highlighted in boldface for these slices.

Figure 4 illustrates the distributions of all the measured parameters of cancerous and healthy slices included in the statistical analysis. The distributions of *B/A*, speed of sound and attenuation at the second harmonic of 2.1 MHz do not significantly differ, while those of the attenuation coefficients at the fundamental frequency do significantly differ ($p < 0.05$). The median *B/A* of cancer is 7.8 versus 7.3 for healthy kidney tissue. The median $\alpha_1$ of cancer is 1.7 dB/cm versus 1.0 dB/cm for healthy kidney tissue.

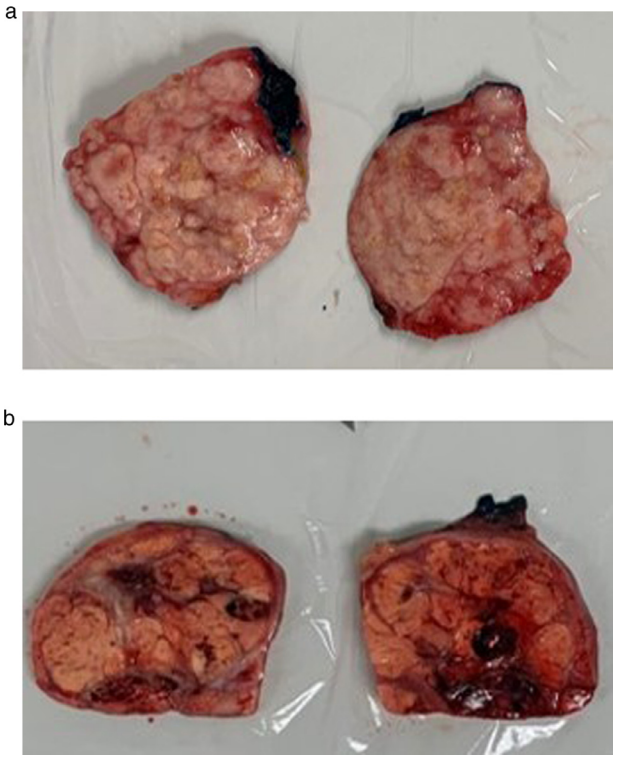


Fig. 3. Tumor slices of kidney samples 1 (a) and 2 (b), exhibiting a macroscopic and microscopic heterogeneous tumor composition with degenerative, fibrotic and edematous changes.

## DISCUSSION

The median *B/A* value of the healthy homogeneous slices is close to the literature value of 6.9 for healthy porcine kidney (Gong et al. 1989). The greater median *B/A* of ccRCC samples may be ascribed to the high lipid and glycogen content characteristic of this tumor (Moch et al. 2016), as fatty tissue has been reported to have high *B/A* values of 10.8−11.0 (Gong et al. 1989). The highly cellular regions of ccRCC also exhibit a significantly lower apparent diffusion coefficient, possibly indicating higher cellular density and lower water content (Squillaci et al. 2004). The latter would also contribute to higher *B/A*. However, statistical analysis of the *B/A* distributions revealed no significant difference between ccRCC and healthy tissue. This may be due to the heterogeneous structure of cancer characterized by fibrotic, degenerative and necrotic changes, confirmed by histology for both samples of ccRCC that exhibited cellular as well as edematous and sclerotic regions. The former are expected to have a lower *B/A* than healthy kidney because of the greater water content in those regions.

The greater median $\alpha_1$ and $\alpha_2$ values for ccRCC compared with healthy tissue are in line with the attenuation observed in optical coherence tomography signals (Freund et al. 2019). We attribute this to the greater composition and structure heterogeneity of malignant tissue that causes scattering and varying phase delays for different acoustic paths within the tissue (Miller et al. 1976; Panfilova et al. 2021b). The difference in attenuation is expected to increase with frequency, because for smaller wavelengths the phase cancelation effects caused by inhomogeneities grow, as observed in our data and in Miller et al. (1976).

The shortcomings of this study include a small sample size, high measurement uncertainty and a possible

Table 3. Measured acoustic parameters of the cancerous tissue slices

| Tumor sample | | | *B/A** | *c* | $\alpha_1$dB/cm | $\alpha_2$dB/cm |
|---|---|---|---|---|---|---|
| Tumor | Slice | Orientation | | | | |
| 1 | 1 | 1 | **7.7 ± 0.9, 8.1 ± 0.9**† | **1517 ± 8** | **0.9 ± 0.0** | **2.5 ± 0.1** |
| 1 | 1 | 2 | **11.9 ± 1.4, 11.4 ± 1.4** | **1516 ± 8** | **0.8 ± 0.0** | **2.2 ± 0.1** |
| 1 | 2 | 1 | **6.7 ± 0.9, 6.7 ± 0.9** | **1565 ± 8** | **1.7 ± 1.0** | **4.2 ± 0.2** |
| 1 | 2 | 2 | **7.3 ± 1, 8.0 ± 1** | **1574 ± 8** | **2.0 ± 1.0** | **5.1 ± 0.3** |
| 1 | 3 | 1 | **7.3 ± 0.6, 7.5 ± 0.6** | **1575 ± 8** | **1.5 ± 0.0** | **3.6 ± 0.1** |
| 1 | 3 | 2 | 0.7 ± 0.6, 0.7 ± 0.6 | **1783 ± 8** | **2.2 ± 0.0** | **6.1 ± 0.2** |
| 2 | 1 | 1 | **10.1 ± 1.1, 10.5 ± 1.1** | **1577 ± 8** | **1.4 ± 0.1** | **4.0 ± 0.2** |
| 2 | 1 | 2 | **9.0 ± 1.5, 9.4 ± 1.5** | **1551 ± 8** | **0.6 ± 0.0** | **2.4 ± 0.2** |
| 2 | 2 | 1 | **8.4 ± 1.0,8.0 ± 1.0** | **1549 ± 8** | **2.4 ± 0.1** | **5.6 ± 0.3** |
| 2 | 2 | 2 | **6.2 ± 1, 6.6 ± 1** | **1560 ± 8** | **1.5 ± 0.1** | **3.8 ± 0.2** |
| 2 | 3 | 1 | **6.8 ± 2, 6.5 ± 2** | **1536 ± 8** | **2.3 ± 0.2** | **8.3 ± 0.7** |
| 2 | 3 | 2 | 17.7 ± 3, 17.9 ± 3 | **1535 ± 8** | **1.6 ± 0.2** | **6.3 ± 0.6** |
| 2 | 4 | 1 | **9.6 ± 1.0, 9.3 ± 1.0** | **1535 ± 8** | **1.7 ± 0.2** | **4.9 ± 0.2** |
| 2 | 4 | 2 | −4.9 ± 1.0, −5.4 ± 1.0 | **1583 ± 8** | **3.9 ± 0.1** | **10.2 ± 0.4** |
| 2 | 5 | 1 | −0.6 ± 1.0, −0.5 ± 1.0 | **1528 ± 8** | **3.4 ± 0.1** | **8.7 ± 0.4** |
| 2 | 5 | 2 | **6.4 ± 1.0,5.9 ± 1.0** | **1531 ± 8** | **2.2 ± 0.1** | **6.2 ± 0.3** |

* The two *B/A* values in each column correspond to two high-amplitude acquisitions.
† Acquisitions that were included in the statistical analysis are presented in boldface.

limitation of the method resulting in inaccurate B/A estimates for highly heterogeneous tissue. The latter two issues are discussed below.

The *B/A* uncertainty of one measurement revealed that the uncertainty in tissue thickness provided the greatest contribution. The range of slice thicknesses used was chosen because it minimized sonic wave attenuation, favoring a better signal-to-noise ratio (SNR). However, the absolute uncertainty of the tissue thickness is equivalent for all measurements and represents the largest percentage of the measurement thickness for thin slices, inducing a greater error. A thickness of ≥6 mm is desired for a low *B/A* measurement uncertainty below ±1.0.

It has been observed that *B/A* values of homogeneous slices exhibit good agreement for the two slice orientations (Table 1; Table 2, kidney 2). At the same time, the measured *B/A* values of visually heterogeneous slices, as illustrated in Figure 2a, varied greatly between two slice orientations, with values uncommon for biological tissue (Table 2, kidney 1). Moreover, uncommon *B/A* values had an augmented corresponding attenuation coefficient at the second harmonic frequency of 4.2 MHz. High attenuation at a frequency of 4.5 MHz, greater than the simulated tissue absorption, was induced by tissue heterogeneity in our *in silico B/A* measurement (Panfilova et al. 2021b), indirectly supporting the observation of the heterogeneity of these slices. As the generalized FAIS assumes the plane wave approximation, the observed variation between two slice orientations and unrealistic values suggests that the tissue slice was too heterogeneous for the plane wave approximation to be valid, causing different parts of the wave front to travel at different speeds of sound. It is of note that measuring the *B/A* of tissue regions with a complicated structure (*e.g.,* boundary of two tissue types) also yielded

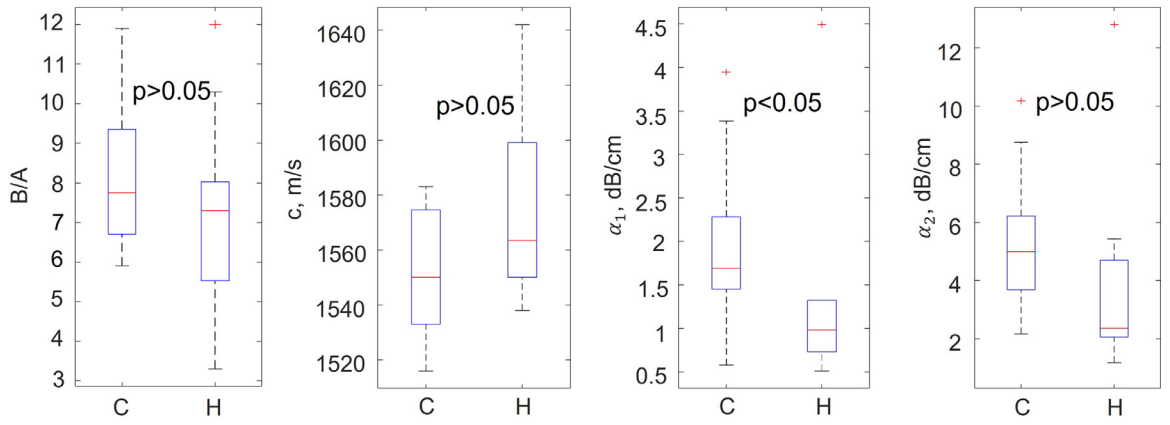


Fig. 4. Acoustic parameters of the cancerous (C) versus healthy (H) tissue slices.

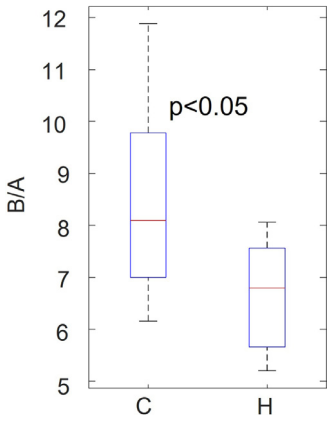


Fig. 5. *B/A* values of the cancerous (C) versus healthy (H) tissue slices, including measurements in agreement for two slice orientations.

abnormal *B/A* values for other researchers (Saito and Kim 2011, Fig. 7). The measurement accuracy may be improved with a smaller region of investigation, leading to less heterogeneity within this region and better agreement between the two slice orientations. One-to-one histopathologic correlation (Muller et al. 2017) of the studied regions and histopathological quantification of the volumes of edematous and cellular regions of the studied slices would yield better understanding of the effect of tissue structure and content on *B/A*.

Provided that the same tissue region is studied and the assumptions of the method are not violated, *B/A* estimates should match within the calculated uncertainty for the two slice orientations. Following this reasoning, *B/A* estimates that do not fulfill this condition could be disregarded as potentially violating the assumptions required for an accurate measurement. With this approach to data analysis, the distributions of *B/A* of ccRCC and healthy tissue are significantly different (Fig. 5), with median values of 8.1 for ccRCC and 6.1 for healthy tissues. However, the uncertainty of the measured *B/A* values must be reduced to prove *B/A* useful for tissue discrimination. The weak point of this approach to data analysis is that the positioning of the sample in two slice orientations was based only on visual observation, and the sonicated region may not be exactly the same.

## CONCLUSIONS

In this work, ccRCC was found to be characterized by a higher median *B/A* and acoustic attenuation and a lower speed of sound than healthy kidney. Only the distributions of the attenuation coefficient at the fundamental frequency of 2.1 MHz differed significantly for ccRCC and healthy kidney. An alternative data analysis indicated *B/A* was significantly different. Because of the small sample size and limitations of the study design, discussed above, the current work cannot provide a definitive conclusion on the utility of the measured parameters for cancer diagnostics.

The current work provides guidance for further experimental studies investigating the utility of *B/A* for cancer diagnostics. In some animal studies, *B/A* has been found to provide better tissue discrimination, compared with linear parameters, attenuation and density (Zhang et al. 2001), opening new possibilities for cancer diagnostics with ultrasound. However, *B/A* echo-mode tissue imaging is a very challenging task (Panfilova et al. 2021a). Therefore, it is important to prove the clinical value of *B/A* in simpler *ex vivo* experiments before further developing this imaging modality.

*Acknowledgments*—This research was supported by the Eindhoven MedTech Innovation Center and in part by the Russian Science Foundation under Grant No. 19-12-00148 (O.A.S.).

## REFERENCES

Apfel RE. Prediction of tissue composition from ultrasonic measurements and mixture rules. J Acoust Soc Am 1986;79:148–152.
Duck FA. Nonlinear acoustics in diagnostic ultrasound. Ultrasound Med Biol 2002;28:1–18.
Freund JE, Buijs M, Savci-Heijink CD, de Bruin DM, de la Rosette JJMCH, van Leeuwen TG, Laguna MP. Optical coherence tomography in urologic oncology: A comprehensive review. SN Compr Clin Med 2019;1:67–84.
Gong X, Zhu Z, Shi T, Huang J. Determination of the acoustic nonlinearity parameter in biological media using FAIS and ITD methods. J Acoust Soc Am 1989;86:1–5.
Jafarzadeh E, Amini MH, Sinclair AN. Determination of the ultrasonic non-linearity parameter *B/A* versus frequency for water. Ultrasound Med Biol 2021;47:809–819.
Janiszewska M, Primi MC, Izard T. Cell adhesion in cancer: Beyond the migration of single cells. J Biol Chem 2020;295:2495–2505.
Law WK, Frizzell LA, Dunn F. Determination of the nonlinearity parameter *B/A* of biological media. Ultrasound Med Biol 1985;11:307–318.
Meyer VR. Measurement uncertainty. J Chromatogr A 1989;1158:15–24.
Miller JG, Yuhas DE, Mimbs JW, Dierker SB, Busse LJ, Laterra JJ, Weiss AN, Sobel BE. Ultrasonic tissue characterization: Correlation between biochemical and ultrasonic indices of myocardial injury. Proc IEEE Int Ultrason Symp 1976;33–43.
Moch H, Humphrey PA, Ulbright TM. WHO classification of tumours of the urinary system and male genital organs. WHO classification of tumours of the urinary system and male genital organs. Lyon: IARC Press; 2016.
Muir TG, Carstensen EL. Prediction of nonlinear acoustic effects at biomedical frequencies and intensities. Ultrasound Med Biol 1980;6:345–357.
Muller BG, Swaan A, de Bruin D, van den Bos W, Schreurs AW, Faber DJ, Zwartkruis ECH, Rozendaal L, Vis AN, Nieuwenhuijzen JA, van Moorselaar RJA, van Leeuwen TG, de la Rosette JJMCH. Customized tool for the validation of optical coherence tomography in differentiation of prostate cancer. Technol Cancer Res Treat 2017;16:57–65.
Panfilova A, Chen X, van Sloun RJG, Wijkstra H, Sapozhnikov OA, Mischi M. The generalized finite amplitude insert-substitution method for *B/A* measurement of tissues and liquids. Proc Mtgs Acoust 2020;42 020001.
Panfilova A, van Sloun RJG, Wijkstra H, Sapozhnikov OA, Mischi M. A review on *B/A* measurement methods with a clinical perspective. J Acoust Soc Am 2021a;149:2200–2237.

Panfilova AP, van Sloun RJG, Wijkstra H, Mischi M. Simulation study on practical choices for *B/A* measurement by the generalized finite amplitude insert-substitution method. Proc IEEE Int Ultrason Symp 2021;2200–2208.

Penet MF, Kakkad S, Wildes F, Bhujwalla ZM. Water and collagen content are high in pancreatic cancer: Implications for quantitative metabolic imaging. Front Oncol 2021;10:3189.

Saito S, Kim JH. Two-dimensional measurement of the nonlinearity parameter *B/A* in excised biological samples. Rev Sci Instrum 2011;82:1–9.

Sehgal CM, Bahn RC, Greenleaf JF. Measurement of the acoustic nonlinearity parameter *B/A* in human tissues by a thermodynamic method. J Acoust Soc Am 1984;76:1023–1029.

Sehgal CM, Brown GM, Bahn RC, Greenleaf JF. Measurement and use of acoustic nonlinearity and sound speed to estimate composition of excised livers. Ultrasound Med Biol 1986;12:865–874.

Squillaci E, Manenti G, Di Stefano F, Miano R, Strigari L, Simonetti G. Diffusion-weighted MR imaging in the evaluation of renal tumours. J Exp Clin Cancer Res 2004;23:39–46.

Wang H, Zhu X, Gong X, Zhang D. Computed tomography of the acoustic nonlinearity parameter *B/A* for biological tissues via difference frequency wave from a parametric array in reflection mode. Chin Sci Bull 2003;48:2427–2430.

Woolson RF. Wilcoxon signed-rank test. Wiley encyclopedia of clinical trials. New York: Wiley; 2007. p. 1–3.

Zeqiri B, Cook A, Rétat L, Civale J, ter Haar G. On measurement of the acoustic nonlinearity parameter using the finite amplitude insertion substitution (FAIS) technique. Metrologia 2015;52:406–422.

Zhang D, Gong X. Experimental investigation of the acoustic nonlinearity parameter tomography for excised pathological biological tissues. Ultrasound Med Biol 1999;25:593–599.

Zhang J, Kuhlenschmidt MS, Dunn F. Influences of structural factors of biological media on the acoustic nonlinearity parameter *B/A*. J Acoust Soc Am 1991;89:80–91.

Zhang D, Gong X, Chen X. Experimental imaging of the acoustic nonlinearity parameter *B/A* for biological tissues via a parametric array. Ultrasound Med Biol 2001;27:1359–1365.